International Journal of Modern Physics B

MAGNETO-SPECTROSCOPY OF EPITAXIAL GRAPHENE

M.L. SADOWSKI*, G. MARTINEZ*, M. POTEMSKI*, C. BERGER†,‡ and W.A. DE HEER†

*Grenoble High Magnetic Field Laboratory, CNRS
25 avenue des Martyrs, 38042 Grenoble, France
sadowski@cnrs.grenoble.fr

†Georgia Institute of Technology,
Atlanta, Georgia, USA

‡ LEPES, CNRS,
Grenoble, France

Received Day Month Year
Revised Day Month Year

We present a far infrared investigation of the optical transitions in epitaxial graphene subjected to a perpendicular magnetic field. Cyclotron-resonance-like transitions between adjacent electron Landau levels are observed, as well as interband transitions. The results are discussed in terms of existing theoretical models of Dirac fermions in graphene, and the relevant optical selection rules.

Keywords: Graphene; magneto-spectroscopy; Landau levels.

1. Introduction

The interest in two-dimensional graphite is fuelled by its particular band structure and ensuing dispersion relation for electrons, leading to numerous differences with respect to "conventional" two-dimensional electron gases (2DEG). Single graphite layers (graphene) have long been used as a starting point in band structure calculations of bulk graphite[1,2,3] and, more recently, carbon nanotubes[4]. The band structure of graphene is considered to be composed of cones located at two inequivalent Brillouin zone corners at which the conduction and valence bands merge. In the vicinity of these points the electron energy depends linearly on its momentum, which implies that free charge carriers in graphene are governed not by Schrödinger's equation, but rather by Dirac's relativistic equation for zero rest mass particles, with an effective velocity $\tilde{c}$, which replaces the speed of light [5,6].

The recent appearance of single graphite layers (graphene), obtained by epitaxial[7,8,9] and exfoliation techniques[10], and the ensuing discovery of an unusual sequence of quantum Hall states[11,12], confirming theoretical predictions[13], has reignited this interest. Holding out prospects of studying quantum electrodynamics in solid state experiments on the one hand and of possible future applications in

novel electronic devices on the other, graphene is currently attracting much interest both on the fundamental and applied levels. However, the extremely small lateral dimensions ($\approx 10\mu$m) of the graphene flakes used in the above-mentioned transport experiments makes them difficult for far infrared transmission measurements. Epitaxial methods on the other hand offer the opportunity of obtaining relatively large, high quality two-dimensional graphite. In the following, we present optical measurements of the characteristic dispersion relation of graphene, confirming directly its expected linear ("relativistic") character.

2. Samples and experiment

The experiments were performed on graphene layers grown in vacuum by the thermal decomposition method [9,14] on single crystal (4H) SiC. These epitaxial graphene structures are routinely characterized using low energy electron diffraction, Auger electron spectroscopy, X-ray diffraction, scanning tunnelling microscopy and atomic force microscopy. The results of these measurements in combination with angular resolved photoelectron spectroscopy and transport data indicate that the active part of this type of structures consists of a few (3-5) graphene layers.

The far infra-red transmission of the samples was measured, at a temperature of 2K, as a function of the magnetic field B. A Si bolometer was placed directly beneath the sample to detect the transmitted radiation. The light (provided and analyzed by a Fourier transform spectrometer) was delivered to the sample by means of light-pipe optics. All experiments were performed with non-polarized light, in the Faraday geometry with the wave vector of the incoming light parallel to the magnetic field direction. The transmission spectra were normalized by the transmission of the substrate and by the zero-field transmission, thus correcting for magnetic field induced variations in the response of the bolometer.

3. Experimental results

A representative transmission spectrum taken at a magnetic field of 0.4 T is shown in Fig. 1. The high energy cut-off of the spectrum is due to the SiC substrate, which was completely opaque for energies between 85 meV (start of the Reststrahlen band in SiC) and about 200 meV. Four lines of various intensities (labelled A - D in the figure) are clearly visible in the spectrum. The process of normalising the spectra by the transmission of an identical substrate ensures that these lines originate from the graphene layer. All the observed lines shift to higher energy with increasing magnetic field. Figure 2 shows the evolution of two of the lines (B and C) with magnetic field. It may be seen that, as the magnetic field increases, both lines shift to higher energy and exhibit a marked increase of intensity. Of the other two lines shown in Fig. 1, line B exhibits a behaviour similar to line C, while line A, inversely, grows weaker with magnetic field and is not observed at higher fields. More lines become visible at higher energies (above the region of substrate opacity) and higher magnetic fields, while at still lower energies than those shown a very wide structure

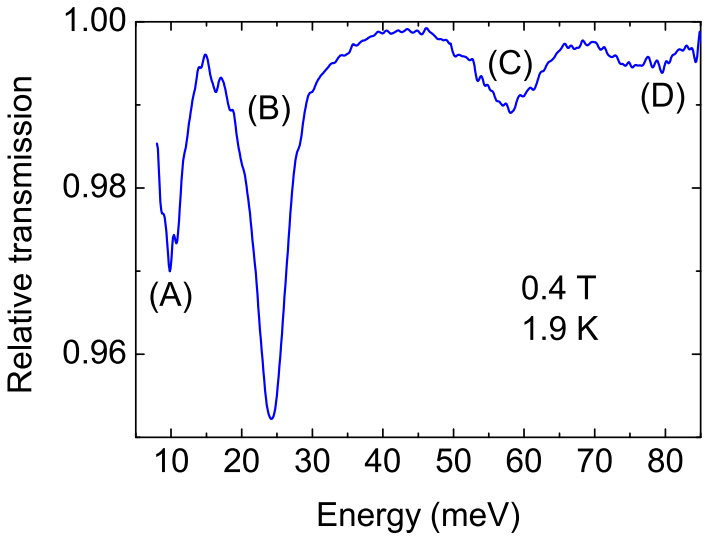

Fig. 1. Transmission spectrum of epitaxial graphene at 0.4 T.

becomes apparent, also moving to higher energies with the magnetic field, but much less rapidly. The line labelled C in Fig. 1 can also be found on the high energy side of the opaque region (see upper panel of Fig. 2).

The positions of all the observed lines are plotted as a function of the square root of the magnetic field in Fig. 3. It may be seen that all the transitions shown in Fig. 1 follow a linear dependence on the square root of the magnetic field. The filled symbols correspond to data taken in a tilted field configuration (50°); the magnetic field plotted in this case is the component perpendicular to the graphene plane. The transition energy is seen to follow the cosine law. The inset to the figure shows the positions of lines C and D, as well as other (weaker) transitions, observed in the higher energy region above 200 meV. These transitions also trace straight lines on the plot.

4. Discussion

In a simple approximation our system may be considered to consist of 2DEG located between the vacuum and a dispersionless polar medium (SiC), characterised by a refractive index n. The transmission of such a system may be shown to be

$$T_{\pm}(\omega) = \frac{16n^2}{|a_{\pm}exp(-i|\vec{k}|d) - b_{\pm}exp(i|\vec{k}|d)|^2} \tag{1}$$

where d is the thickness of the substrate, $\vec{k}$ is the wavevector, the $\pm$ sign corresponds to right- and left-handed circular polarisations, $a_{\pm} = (n+1)(n+1+\sigma_{\pm}(\omega, B))$, $b_{\pm} = (n-1)(n-1-\sigma_{\pm}(\omega, B))$ and all the relevant information is contained in

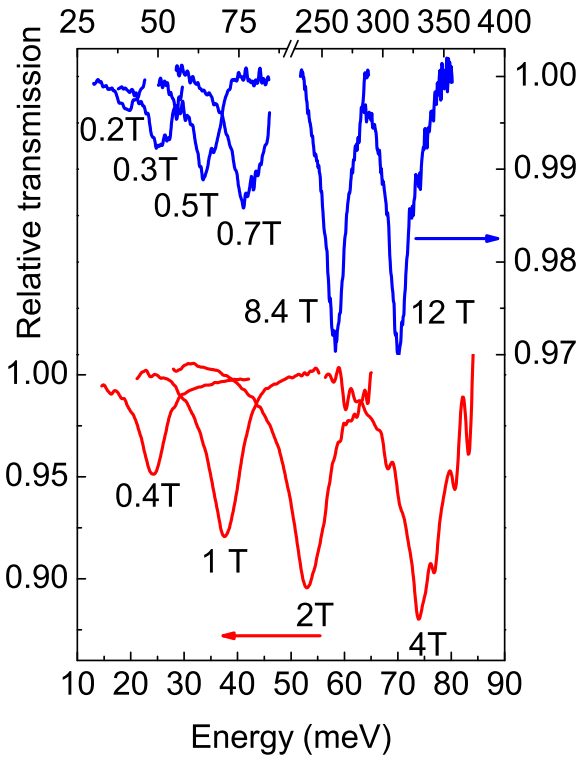

Fig. 2. Evolution of two of the observed lines with magnetic field. The upper panel shows the line labelled C in Fig. 1, while the lower panel shows line B. Note the increase in intensity of both lines.

the dynamic conductivity tensor $\sigma_{\pm}(\omega, B) = \sigma_{xx}(\omega, B) \pm i\sigma_{xy}(\omega, B)$. The above expression may be simplified by averaging out over the interferences in the plane-parallel slab of the substrate to yield

$$T_{\pm}(\omega) = \frac{16n^2}{|a_{\pm}|^2 - |b_{\pm}|^2} \tag{2}$$

In the limit of weak absorption and normalised by the transmission of a substrate without the 2DEG, this may be further simplified to

$$T_{\pm}(\omega) \simeq 1 - \frac{(n^2+3)}{2(n^2+1)} \frac{Re(\sigma_{\pm}(\omega, B))}{\epsilon_0 c} \tag{3}$$

The optical conductivity tensor of a graphene layer in a magnetic field is a complicated and cumbersome quantity to evaluate[15,16]. In a simple way however, it may be obtained directly by using the Kubo-Greenwood formalism and introducing a purely phenomenological line broadening. We write

$$\sigma_{\pm}(\omega, B) = \frac{4G_B e^2}{\omega} \sum_{m,n} \frac{(f_n - f_m)}{E_m - E_n - (\hbar\omega + i\gamma)} \langle n|\hat{v}_{\pm}|m\rangle\langle m|\hat{v}^*_{\pm}|n\rangle \tag{4}$$

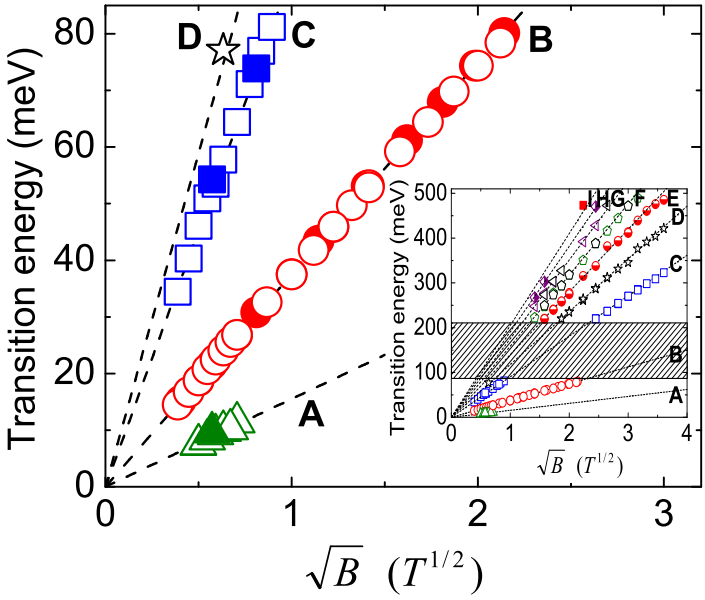

Fig. 3. Evolution of the observed transmission with magnetic field. Filled symbols correspond to a tilted field configuration. The inset shows the positions of transitions in a wider energy range. The shaded region corresponds to the spectral range where the substrate is opaque.

where E_m, E_n are the energies of Landau levels m and n, $G_B = eB/h$ is the magnetic-field-induced Landau level degeneracy, f_m, f_n are the occupancies of the relevant Landau levels and the factor 4 accounts for the spin and valley degeneracies. The summation is performed over all Landau levels m, n. The velocity operators $\hat{v}_\pm = \frac{1}{\sqrt{2}}(\hat{v}_x \pm i\hat{v}_y)$, where $\hat{v}_x$ and $\hat{v}_y$ are defined by eq. 12, account for the selection rules governing the optically active transitions.

Electrons in graphene sheets have long been described in terms of the relativistic Dirac equation [2,17,5]. Thus, in the vicinity of the Dirac points K and K'

$$E(\vec{k}) = \pm\sqrt{(m_0\tilde{c}^2)^2 + (\tilde{c}|\vec{k}|\hbar)^2} \tag{5}$$

or the usual relationship between energy and momentum. Here $\tilde{c}$ is a parameter with velocity units, mimicking the speed of light in the relativistic formulation of the problem. Physically, $\tilde{c}$ is a measure of the interactions between nearest neighbours in the graphene lattice, and is obtained as $\tilde{c} = (\sqrt{3}/2)a_0\gamma_0/\hbar$, where γ_0 is the energy overlap between neighbouring atoms, $\gamma_0 \simeq 3.16$ eV[18] and $a_0 = 1.42\mathring{A}$ is the distance between them. The quantity m_0 may be interpreted as the effective rest mass of the electron (quasiparticle), or - equivalently - as the energy gap between the valence and conduction bands. This mass is considered to be a result of interactions between neighbouring graphene sheets[5]; in the ideal case of pure graphene the effective rest mass m_0 is zero and $E(\vec{k}) = \pm\tilde{c}\hbar|\vec{k}|$. This is the case we shall consider in the

following, and not distinguish between K and K'.

The wavefunctions corresponding to the Landau levels are bi-spinors; following Ando[4] we shall write them in the form

$$F_n = \frac{1}{\sqrt{2}} \begin{pmatrix} sgn(n) h_{|n|-1} \\ h_{|n|} \end{pmatrix} \quad for \quad n \neq 0; \quad F_0 = \begin{pmatrix} 0 \\ h_0 \end{pmatrix} \tag{6}$$

where the functions $h_n(x, y)$ are defined by

$$h_n(x, y) = \frac{(\hat{a}^\dagger)^n}{\sqrt{n!}} h_0(x, y) \tag{7}$$

with $\hat{a} h_0(x, y) = 0$. The lowering and raising operators $\hat{a}$ and $\hat{a}^\dagger$ are defined as

$$\hat{a} = \left(\sqrt{\frac{\hbar}{2eB}} \right) (\hat{\pi}_x - i\hat{\pi}_y) \quad \hat{a}^\dagger = \left(\sqrt{\frac{\hbar}{2eB}} \right) (\hat{\pi}_x + i\hat{\pi}_y) \tag{8}$$

with $\hat{\pi}_x = -i\partial/\partial x + e/\hbar A_x$, $\hat{\pi}_y = -i\partial/\partial y + e/\hbar A_y$ and $\mathbf{A}$ the vector potential. The following relations are then satisfied

$$\hat{a}^\dagger h_n = \sqrt{n+1} h_{n+1} \quad \hat{a} h_{n+1} = \sqrt{n+1} h_n \quad \hat{a}^\dagger \hat{a} h_n = n h_n \tag{9}$$

The Hamiltonian may be simply written as

$$\hat{H}_0 = E_1 \begin{pmatrix} 0 & \hat{a} \\ \hat{a}^\dagger & 0 \end{pmatrix} \tag{10}$$

where E_1 is a characteristic energy (the energy of the first Landau level), $E_1 = \tilde{c}\sqrt{2e\hbar B}$. The eigenenergies - energies of Landau levels - are then given by

$$E_n = sgn(n) E_1 \sqrt{\mid n \mid} \tag{11}$$

Note that the Landau level corresponding to $n = 0$ is special in that it is both an electron and a hole level, and its energy does not change with the magnetic field.

The velocity operators $\hat{v}_x, \hat{v}_y$ are defined by the commutators

$$\hat{v}_x = \frac{1}{i\hbar}[x, \hat{H}] = \tilde{c} \begin{pmatrix} 0 & 1 \\ 1 & 0 \end{pmatrix}, \quad \hat{v}_y = \frac{1}{i\hbar}[y, \hat{H}] = \tilde{c} \begin{pmatrix} 0 & -i \\ i & 0 \end{pmatrix} \tag{12}$$

We may then calculate the matrix elements in eq. 4:

$$\langle n|\hat{v}_+|m\rangle\langle m|\hat{v}_+^*|n\rangle = \tilde{c}^2 h_{|n|-1}^2 h_{|m|}^2 = \frac{\tilde{c}^2}{2} \delta_{|n|-1,|m|} \tag{13}$$

$$\langle n|\hat{v}_-|m\rangle\langle m|\hat{v}_-^*|n\rangle = \tilde{c}^2 h_{|n|}^2 h_{|m|-1}^2 = \frac{\tilde{c}^2}{2} \delta_{|n|,|m|-1} \tag{14}$$

for transitions involving Landau levels L_n with $n \neq 0$, and

$$\langle n|\hat{v}_+|0\rangle\langle 0|\hat{v}_+^*|n\rangle = 2\tilde{c}^2 h_0^2 h_{|n|-1}^2 = \tilde{c}^2 \delta_{0,|n|-1} \tag{15}$$

$$\langle 0|\hat{v}_-|n\rangle\langle n|\hat{v}_-^*|0\rangle = 2\tilde{c}^2 h_0^2 h_{|n|-1}^2 = \tilde{c}^2 \delta_{0,|n|-1} \tag{16}$$

$$\langle 0|\hat{v}_+|n\rangle\langle n|\hat{v}_+^*|0\rangle = 0 \tag{17}$$

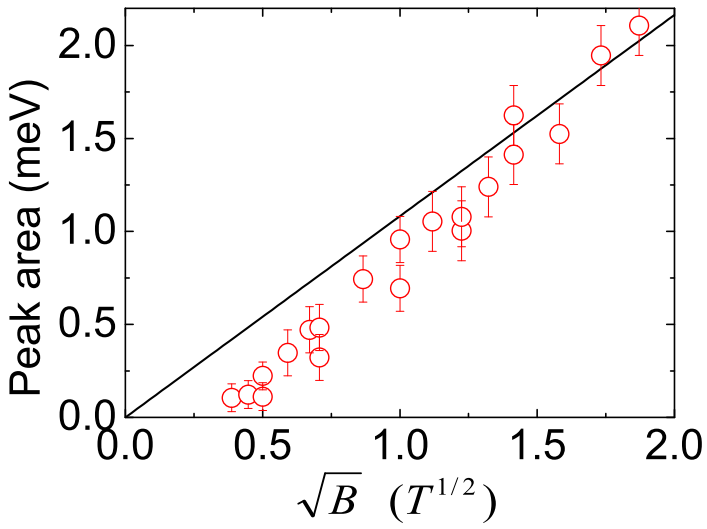

Fig. 4. Oscillator strength of the $L_0 \rightarrow L_1$ transition in graphene plotted against the square root of the magnetic field.

$$\langle n|\hat{v}_-|0\rangle\langle 0|\hat{v}_-^*|n\rangle = 0 \tag{18}$$

for those involving the L_0 level.

The optical selection rules thus allow transitions from $L_n \rightarrow L_m$ such that $|m| = |n| - 1$ for the "+" polarisation (eqs. 13,15,17) and $|m| = |n| + 1$ in the "-" polarisation (eqs. 14, 16, 18). For unpolarised radiation, used in the current experiment, the allowed transitions are simply those between states n, m such that $|m| = |n| \pm 1$.

We note that according to eq. 11, the allowed transitions are expected to occur at energies $\Delta_n = E_1(\sqrt{|n|} \pm \sqrt{|n|-1})$. We further note that, using unpolarised radiation, it is not possible to distinguish between pairs of transitions where the indices n and m have different signs, such as $L_{-1} \rightarrow L_0$ and $L_0 \rightarrow L_{-1}$, $L_{-1} \rightarrow L_2$ and $L_{-2} \rightarrow L_1$, and so on. Physically, this symmetry arises from the fact that electron and hole states are constructed from the same atomic orbitals. In view of the above we assign the strongest line visible in Fig. 1 - marked B - to the two transitions involving the zero-th Landau level L_0. The slope of its dependence on the square root of the magnetic field is $\tilde{c}\sqrt{2e\hbar}$, which allows us to determine the value of the only independent parameter, $\tilde{c}$, as being equal to 1.03 $\times 10^6$ m/s, with an accuracy of 0.01 m/s. With this value, all the other possible transitions may be immediately identified. The transition marked A corresponds to a slope of $\tilde{c}\sqrt{2e\hbar}(\sqrt{2} - \sqrt{1})$, which is the transition $L_1 \rightarrow L_2$. Line C has a slope of $\tilde{c}\sqrt{2e\hbar}(\sqrt{2} + \sqrt{1})$, which is the pair of transitions $L_{-1} \rightarrow L_2$ and $L_{-2} \rightarrow L_1$. The higher energy lines are found at positions corresponding to the sums of the square roots of consecutive integers, thus: D - $\tilde{c}\sqrt{2e\hbar}(\sqrt{3} + \sqrt{2})$, transitions $L_{-2} \rightarrow L_3$ and $L_{-3} \rightarrow L_2$, E -

$\tilde{c}\sqrt{2e\hbar}(\sqrt{4}+\sqrt{3})$, transitions $L_{-3} \rightarrow L_4$ and $L_{-4} \rightarrow L_3$, etc. We stress again that the energies of all the transitions are determined by a single parameter, the velocity $\tilde{c}$, which has always been taken to be $\sim 10^6$ m/s - a value recently confirmed by transport experiments[11,12,14].

While for a conventional 2DEG, with a quadratic dispersion law, there is a coincidence between classical and quantum mechanical solutions of the optically active response in a magnetic field, this does not hold for graphene. The classically derived cyclotron excitation E_C in this system is $E_C = \hbar eB/(E/\tilde{c}^2)^6$, where E is the electron energy and $(E/\tilde{c}^2)$ stands for the electron mass - energy and mass being equivalent in the relativistic picture. Although the effective rest mass of the electrons in graphene is zero, they have a non-zero, energy-dependent cyclotron mass which is also a function of the magnetic field. The line marked A in Figs. 1-3, corresponding to the transition between Landau levels 1 and 2: $L_1 \rightarrow L_2$, allows to determine the effective mass in the range of energies observed as changing from 0.002 m_0 to 0.007 m_0.

It should be mentioned that cyclotron resonance in bulk graphite has been studied both experimentally[19] and theoretically[20,21]. Although the resonant magnetic field for a given energy was also found to scale with the cosine of the angle between the field and the graphene planes, in contrast to our findings these experiments were well described by a conventional linear dependence of the cyclotron frequency ω_C on the magnetic field, with an effective mass of 0.058 m_0.

The other observed lines correspond to interband transitions, or electron-positron creation and annihilation in the relativistic picture. It is noteworthy that all these transitions are also in perfect agreement with a single-particle model, and there is no sign of electron-electron interactions. The strongest transition, involving the zero Landau level L_0, is unique in that it may be considered simultaneously an interband transition, an electron cyclotron resonance transition and a hole cyclotron resonance transition, the L_0 Landau level being both an electron and a hole level.

For the case of unpolarised radiation, eq. 3 may be rewritten as

$$T(\omega) = \frac{1}{2}(T_+(\omega) + T_-(\omega)) =\simeq 1 - \frac{(n^2+3)}{2(n^2+1)} \frac{Re(\sigma_{xx}(\omega, B))}{\epsilon_0 c} \tag{19}$$

The integrated transmission for a single transition between a completely filled (L_0) and a completely empty (L_1) Landau level, using the above expression (for linewidths γ small compared to the transition energy) may be written as:

$$I(B) = \frac{1}{\epsilon_0 c} \int Re(\sigma_{xx}(\omega, B)) d\omega \approx \frac{(n^2+3)}{2(n^2+1)} \frac{e^3 \tilde{c} B}{\epsilon_0 c E_1} = \frac{(n^2+3)}{2(n^2+1)} \frac{e^2}{2\epsilon_0 \hbar c} E_1 \tag{20}$$

where E_1 is the characteristic energy introduced earlier.

The above equation gives a rough estimate of the intensity of the strongest transition, in the range of high magnetic fields where the Fermi energy is pinned to the L_0 level. This is due to the fact that the decreasing intensity of the $L_0 \rightarrow L_1$ transition is compensated by the corresponding increase of the strength of the

superimposed $L_{-1} \rightarrow L_0$ transition. In spite of the rather crude approximation, Fig. 4 indeed shows that the observed transition follows the expected trend.

The fact that transitions involving the L_0 Landau level are visible at such low magnetic fields places an upper limit on the Fermi energy and thus the electron concentration in the observed layer. The observation of the $L_0 \rightarrow L_1 (L_{-1} \rightarrow L_0)$ line implies the existence of unpopulated states at least on the L_1 level. This line is clearly observed at fields $B \approx 0.15$ T, and therefore the L_1 level can be fully populated only when $B < 0.15$ T. Thus $n \leq 2.1 \times 10^{10}$ cm^{-2} (where we take into account the 2- and 4-fold degeneracy of the L_0 and L_1 electronic Landau levels, respectively).

On the other hand, a mesoscopic sample patterned on the same wafer as our sample has been investigated in transport experiments which also show the unusual quantum Hall effect in epitaxial graphene. These measurements yield a sheet concentration of $\simeq 4 \times 10^{12}$ cm^{-2}. This concentration discrepancy may be explained as follows. As usual at the interfaces, the electric field induced by the surface charge compensates for the work function difference between SiC and graphene. Due to the abrupt change of the built-in electric field, the interface monolayer has a high carrier concentration, which decreases away from the interface: while the Fermi energy in the first monolayer is located high in the conduction band, it may be quite close to the Dirac point for other layers. It is believed that these transport experiments probe the interface layer in which the estimated electron sheet concentration is high; in contrast, our transmission experiments probe the whole sequence of layers, among them also those which are quasi-neutral. The previously mentioned very low-energy features in our spectra probably arise from the high-electron-concentration parts of the sample, where the energy difference between adjacent Landau levels is small.

Another factor possibly affecting the data could be lateral inhomogeneity, i.e. fluctuations in the electron concentration, within a single graphene plane. Finally, individual graphene planes in epitaxial graphite may be much more weakly coupled than is usually accepted for graphite – evidence for weaker coupling has been found in nano-graphene layers on graphite substrates[22]. The current experiment shows an absorption in good agreement with that expected for graphene, but the simple approximation used may be insufficient to definitely distinguish between one and a few (inhomogeneous) uncoupled layers.

5. Conclusions

Concluding, we have measured the optical excitation spectrum of Dirac fermions in a condensed matter system. These fermions are found in thin layers of epitaxial graphite, most probably in the form of single (or extremely weakly coupled) graphene layers (or parts of layers). These excitations are very well described in terms of a relativistic-like Dirac hamiltonian. Cyclotron resonance-like transitions coexist with interband (particle-antiparticle)-like transitions, with energy positions and oscillator strengths in surprisingly good agreement with expectations based on

a model of non-interacting particles with linear dispersion.

The GHMFL is a "Laboratoire conventionné avec l'UJF et l'INPG de Grenoble". The present work was supported in part by the European Commission through grant RITA-CT-2003-505474 and by grants from the Intel Research Corporation and the NSF: NIRT "Electronic Devices from Nano-Patterned Epitaxial Graphite".

References

1. P.R. Wallace, *Phys. Rev.* **71**, 622 (1947)
2. J.W. McClure, *Phys. Rev.* **104**, 666 (1956)
3. J.C. Slonczewski and P.R. Weiss, *Phys. Rev.***109**, 272 (1958)
4. T. Ando, *J. Phys. Soc. Jpn.* **74**, 777 (2005)
5. F.D.M. Haldane, *Phys. Rev. Lett.* **61**, 2015 (1988)
6. Y. Zheng and T. Ando, *Phys. Rev. B* **65**, 245420 (2002)
7. I. Forbeaux, J.-M. Themlin, and J.-M. Debever, *Phys. Rev. B* **58**, 16396 (1998)
8. A.Charrier, A. Coati, T. Argunova, F. Thibaudau, Y. Garreau, R. Pinchaux, I. Forbeaux, J.-M. Debever, M. Sauvage-Simkin, J.-M. Themlin, *J. Appl. Phys.* **92**, 2479 (2002)
9. C. Berger, Z. Song, T. Li, X. Li, A.Y. Ogbazghi, R. Feng, Z. Dai, A.N. Marchenkov, E.H. Conrad, P.N. First, and W.A. de Heer, *J. Phys. Chem.* **108**, 19912 (2004).
10. K.S. Novoselov, A.K. Geim, S.V. Morozov, D. Jiang, Y. Zhang, S.V. Dubonos, I.V. Grigorieva, and A.A. Firsov, *Science* **306**, 666 (2004)
11. K.S. Novoselov, A.K. Geim, S.V. Morozov, D. Jiang, M.I. Katsnelson, I.V. Grigorieva, S.V. Dubonos, A.A. Firsov, *Nature* **438**, 197 (2005).
12. Y. Zhang, Y.-W. Tan, H.L. Stormer and P. Kim, *Nature* **438**, 201 (2005).
13. V.P. Gusynin and S.G. Sharapov, *Phys. Rev. Lett.***95**, 146801 (2005).
14. C. Berger, Z. Song, T. Li, X. Li, X. Wu, N. Brown, C. Naud, D. Mayou, A.N. Marchenkov, E.H. Conrad, P.N. First, and W.A. de Heer, *Science* **312**, 1191 (2006)
15. T. Ando, Y. Zheng, and H. Suzuura, *J. Phys. Soc. Jpn.* **71**, 1318 (2002)
16. V.P. Gusynin and S.G. Sharapov, *Phys. Rev. B* **73**, 245411 (2006)
17. M.S. Dresselhaus and G. Dresselhaus, *Advances in Physics* **51**, 1 (2002)
18. W.W. Toy, M.S. Dresselhaus, and G. Dresselhaus, *Phys. Rev.* **15**, 4077 (1977)
19. J.K. Galt, W.A. Yager, and H. W. Dail, Jr., *Phys. Rev.* **103**, 1586 (1956)
20. P. Nozières, *Phys. Rev.* **109**, 1510 (1958)
21. M. Inoue, *J. Phys. Soc. Jpn.* **17**, 808 (1962)
22. A.M. Affoune, B.L.V. Prasad, H. Sato, T. Enoki, Y. Kaburagi, and Y. Hishiyama, *Chem. Phys. Lett.* **348**, 17 (2001)